Sensors and Materials, Vol. 37, No. 5 (2025) 1891–1902
MYU Tokyo

S & M 4026

Residual Stress Sensing in Press-fitting of Low-carbon Steel Components Using X-ray Diffraction Techniques

Shih-Chuan Cheng* and Rong-Shean Lee

Department of Mechanical Engineering, National Cheng Kung University
No. 1, University Road, East District, Tainan City 701, Taiwan (R.O.C.)

(Received January 10, 2025; accepted April 28, 2025)

Keywords: residual stress sensing, X-ray diffraction, press-fitting strain, stress relief, stress measurement

Residual stresses in metal components, particularly in deep-drawn sheet metal parts, can lead to dimensional instability, noise, and premature failure. In this study, we developed a cost-effective approach to residual stress relief by utilizing press-fitting strain—an inherent assembly process—to mitigate internal stresses without requiring additional processing. A nondestructive residual stress sensing method based on X-ray diffraction (XRD) with the $\sin^2\psi$ technique was employed to monitor and evaluate stress variations at multiple locations on low-carbon steel components. The XRD system functions as a precision sensor for detecting internal stress distributions through changes in crystal lattice spacing, providing critical data on stress relief behavior. Experimental results revealed a location-dependent response: while stress increased at regions far from the press-fit zone, a significant reduction was observed directly beneath the press-fitted interface. This highlights the dual role of mechanical interference both as a joining method and an effective in-process stress relief strategy. The findings demonstrate a novel sensing-integrated framework for residual stress measurement in metal forming, supporting future developments in intelligent manufacturing and sensor-based process monitoring systems.

1. Introduction

1.1 Background

Residual stresses in metal parts can cause deformation or warping, which affects their dimensional stability and functionality. Residual stresses often originate from manufacturing processes such as welding, machining, casting, or heat treatment, where uneven cooling or plastic deformation induces internal imbalances. Thin-walled components, forged parts, and geometrically complex structures are particularly susceptible to such changes. Over time, residual stresses may lead to many adverse effects such as structural fatigue; fracture; reduced tensile strength, interface bond strength of coating, and dimensional stability; increased friction, and corrosion under tensile stress.(1,2)

*Corresponding author: e-mail: n18061054@gs.ncku.edu.tw
https://doi.org/10.18494/SAM5540

ISSN 0914-4935 © MYU K.K.
https://myukk.org/

To mitigate these effects, techniques such as stress-relief annealing, vibration, shot peening[3] and deformation[4] can be employed. Monitoring residual stress accurately is essential, and sensing technologies such as X-ray diffraction (XRD) have become widely adopted owing to their nondestructive and highly sensitive measurement capabilities. In particular, XRD-based residual stress sensing allows engineers to detect internal stress distributions through changes in crystal lattice spacing, enabling improved process control and material reliability.

As sensing and material technologies advance, integrating stress sensing into manufacturing and postprocessing has become increasingly important for quality assurance in precision applications. Understanding residual stresses and how to minimize them are critical and require further investigation to improve quality

1.2 Literature review

1.2.1 Review of residual stress

Residual stresses refer to internal stresses remaining within a material after the removal of the original cause. These stresses arise from three primary sources:

1) Thermal Effects: Processes such as welding, casting, and heat treatment cause nonuniform heating and cooling, leading to thermal gradients and residual stresses.[5–7]
2) Mechanical Deformation: Manufacturing processes such as bending, rolling, and machining induce plastic deformation, with adjacent regions preventing full elastic recovery.[8]
3) Assembly and Joining: Techniques involving dissimilar materials or complex geometries, such as welding, create residual stresses from differential expansion and contraction.[6,7,9]

Understanding residual stresses and how to reduce them are critical for improving manufacturing processes and ensuring material reliability.

1.2.2 Review of residual stress relief through deformation

Recent studies have advanced our understanding of residual stress relief through deformation, employing innovative experimental and computational techniques. Ball *et al.* used 3D XRD to study the evolution of residual stresses in ferritic steel under uniaxial deformation.[10] Tracking around 1800 grains, they observed that while residual stresses persisted during plasticity, they diminished with increasing strain. Their study also highlighted the importance of grain orientation and neighborhood effects, as well as the role of the Schmid factor in intergranular stress evolution. Tagiltsev and Shutov developed a geometrically nonlinear model to analyze viscoplastic structures with residual stresses, particularly in welded plates.[11] Using finite element simulations, they demonstrated the model's capability to predict and manage residual stresses in complex systems. These studies collectively reveal how deformation history, microstructural interactions, and advanced modeling can help predict and mitigate residual stresses, improving material performance in applications ranging from amorphous solids to steel and welded structures. According to Robinson *et al.*, cold compression effectively relieves residual stresses in aluminum 7075 by redistributing internal stresses through controlled plastic deformation, reducing tensile stresses in the core and compressive stresses near the surface.(12) Immediate application of cold compression after quenching enhances stress relief by preventing significant natural aging. Delayed cold compression allows solute clustering and material hardening, reducing its effectiveness.

1.3 Study of press-fitting strains for reducing residual stresses

Although there are many techniques for reducing residual stresses especially those caused by deformation, all extra processes will incur cost. As press-fitting is the postprocess for deep-drawn sheet metal components, utilizing the interference level (strain) can be a self-serving problem-solving method to reduce residual stresses without extra cost. However, methods using assembly interference have not yet been identified for residual stress reduction. In this study, we performed experiments and measured the changes in residual stresses with respect to different strains by press-fitting at different places on a workpiece to investigate the effects of press-fitting strains on residual stress relief.

2. Measurement of Residual Stresses

2.1 Residual stress measurement techniques

Residual stress measurement is based on the principle that stresses locked within a material cause elastic deformation, which can be detected and quantified through changes in the material's strain, lattice structure, or properties. Some residual stress measurement techniques and sensors used are listed in Table 1. As press-fitting is a permanent fixture and the assembled parts can only be measured by nondestructive measurements, the XRD technique is chosen.

2.2 Stress measurement by XRD

XRD is a powerful technique for measuring residual stresses in materials. This method leverages Bragg's Law to evaluate the strain in crystalline materials and determine the corresponding stresses. The relationship is expressed as

Table 1
Residual stress measurement techniques and sensors used.

Technique	Sensors used	Destructive (D)/ nondestructive (ND)	Reference
Hole drilling	Strain gauges, strain	D	ASTM E837 for hole-drilling method(13)
XRD	X-ray detectors	ND	General XRD techniques and ASTM E915(14)
Neutron diffraction	Neutron detectors	ND	ISO 21432 for neutron diffraction(15)
Ultrasonic methods	Ultrasonic transducers, wave velocity sensors	ND	Gorgun and Karamis(16)

$$n\lambda = 2d\sin\theta, \tag{1}$$

where n is the integer order of diffraction (dimensionless) and λ is the wavelength of the X-rays (Å) (angstroms). In this study, λ = 2.2897 Å for Cr-Kα. d is the interplanar spacing (Å), and θ is the diffraction angle (°). When X-rays strike a crystalline material, they diffract at specific angles corresponding to the material's atomic arrangement.

Residual stress measurement using XRD is based on the principle that residual stresses alter the spacing of atomic planes within a material. Compressive stresses reduce the interplanar spacing, while tensile stresses increase it, leading to measurable shifts in the diffraction angle ($\Delta\theta$). To measure these stresses, a specific set of lattice planes (*hkl*) is selected for analysis, and the sample is tilted or rotated to record diffraction angles (θ) at various orientations (ψ) relative to the surface normal. Changes in θ are used to calculate the strain (ε) in the material, expressed as the change in interplanar spacing due to strain [Δd (Å)] relative to the stress-free value [d_0 (Å)], using the relationship

$$\varepsilon = \frac{\Delta d}{d_0}. \tag{2}$$

The strain is then related to stress (σ, MPa) through the material's elastic constants, such as Young's modulus (E, GPa) and Poisson's ratio (v), using the equation

$$\sigma = \frac{E}{1+\nu}\cdot\varepsilon. \tag{3}$$

By analyzing diffraction data from multiple orientations, we can determine the residual stress tensor, providing a comprehensive understanding of the stress distribution within the material.

2.3 Comparing cosα and sin$^2\psi$ methods

There are two XRD residual stress measurements methods: cosα and sin$^2\psi$. Both measure the change in strain to calculate residual stresses. The measurement principle of the sin$^2\psi$ method is that the stress is proportional to the gradients of $\varepsilon_{\varphi\psi}^{\{hkl\}}$ and sin$^2\psi$, whereas the measurement principle of the cosα method is that the stress is proportional to the gradients of $\varepsilon_{\alpha}^{\{hkl\}}$ and cosα as in Eqs. (4) and (5).[17]

$$\sigma_\varphi = \frac{1}{1/2S_2^{\{hkl\}}}\frac{\partial\varepsilon_{\varphi\psi}^{\{hkl\}}}{\partial\sin^2\psi} \tag{4}$$

$$\sigma_\varphi = \frac{1}{1/2S_2^{\{hkl\}}}\frac{1}{\sin 2\eta\ \sin 2\psi_0}\frac{\partial\varepsilon_{\alpha}^{\{hkl\}}}{\partial\cos\alpha} \tag{5}$$

The detector used for the $\sin^2\psi$ method is a position-sensitive scintillation line detector. It requires multiple sample orientations to capture strain at different ψ angles [tilt angle from the sample normal (°)]. The sampling time for one point is longer as it requires multiple sampling points. The measuring equipment requires a tilting stage and a line detector. The detector used for the cosα method is a 2D photosensitive detector. It is a faster method as it uses a single exposure to collect strain information over the entire diffraction cone. Although $\cos\alpha$ is a later and faster method to measure residual stress, the geometry of the workpiece will interfere with XRD. Hence, we use the 1D $\sin^2\psi$ method to measure the residual stresses at different places on the workpiece.

3. Experimental Methodology

A carbon steel deep-drawn sheet metal component made by multistage stamping forming contains residual stresses from the forming and deep-drawing processes. The material of the sheet metal is as shown in Table 2. The residual stresses of the workpiece are measured before and after press-fitting to evaluate the effect of press-fitting. The experimental flow chart shown in Fig. 1 outlines a systematic process for evaluating the residual stress relief effects of press-fitting on deep-drawn sheet metal components using XRD measurements. The assembly diagram of press-fitting configurations is shown in Fig. 2.

3.1 XRD stress measurement before press-fitting

Before subjecting the deep-drawn component to press-fitting, an XRD analysis is conducted using the Proto iXRD® system to measure residual stresses. As the surface condition will affect the measurement value, we used a 1-mm-diameter collimator to increase data precision. This baseline measurement provides data on stress distribution and material properties prior to the next step. The XRD measurement conditions are as shown in Table 3.

The XRD measurements were carried out using the Proto iXRD® system with a stationary goniometer setup. The system employs a Cr-Kα radiation source with a wavelength of 2.2897 Å

Table 2
Chemical composition of deep draw stamping component of carbon steel (mass% × 1000).

C	Si	Mn	P	S	Fe
2	0	10	10	11	Bal

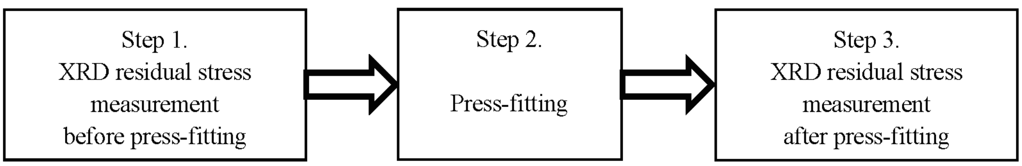

Fig. 1. Experimental methodology.

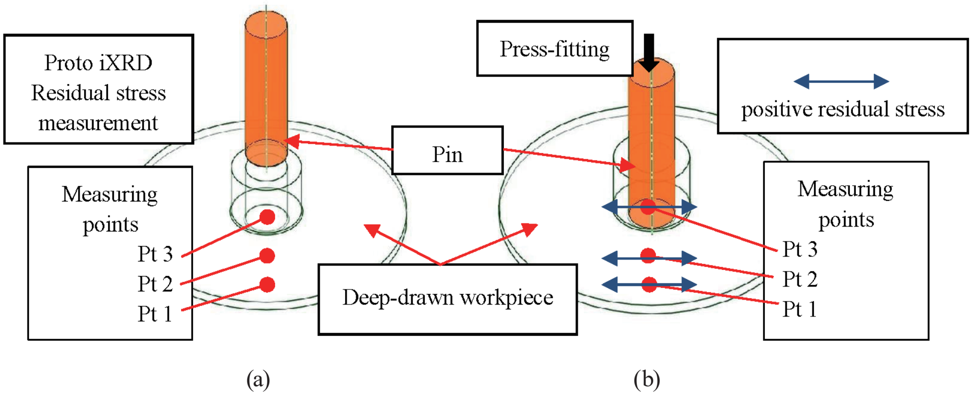

Fig. 2. (Color online) Configuration of specimens and measuring points: (a) before press-fitting and (b) after press-fitting.

Table 3
Stress measurement conditions.

Measured method	$\sin^2\psi$	Tube voltage	25 keV
Tube current	5 mA	Collimator diameter	1 mm
X-ray irradiation angle	45°	X-ray irradiation time	5 s
Characteristic X-ray	Cr-Kα	K-β filter	V
Wavelength	2.2897 Å	2-Theta Angle (Approx.)	156.1°
Bravais lattice	BCC	Diffraction plane	Ferrite {211}
X-ray elastic constant	175 GPa		

and is filtered with a V-type Kβ filter to ensure monochromatic X-rays. The diffraction data were obtained from the {211} planes of BCC ferritic steel, which are sensitive for stress analysis because of their high diffraction intensity and stress response characteristics.

A 1-mm-diameter collimator was used to minimize spot size and improve spatial resolution, particularly suitable for localized measurements on complex geometries such as drawn cups. The ψ-tilt range was set between −25° and +25° in 6.25° increments to ensure accurate fitting for the $\sin^2\psi$ method. The exposure time for each angle was 5 s, resulting in approximately 1–2 min per data point including motorized positioning time.

Data were analyzed using Proto XRDWin software, applying linear regression to the $\sin^2\psi$ plot to determine the slope corresponding to in-plane stress. The X-ray elastic constant (XEC) used for ferritic steel in the {211} plane was 175 GPa, as specified in Proto's calibration data.

3.2 Press-fitting

The radial strain during press-fitting (ε_r, expressed as %) is the change in diameter ($D_{pin} - D_{hole}$, unit in mm) over the original diameter (D_{hole}, unit in mm). The strain equation for axis-symmetric deformation is

$$\varepsilon_r = \frac{D_{pin} - D_{hole}}{D_{hole}}. \tag{6}$$

The component is subjected to press-fitting to alter the stress state of the material due to induced deformation. The material of the pin is as shown in Table 4. It is considered a rigid body. The pin diameter is 2.99 mm. The strain before press-fitting is $\varepsilon_r = 0$. There are three different inner wall diameters used, namely, 2.96, 2.95, and 2.93 mm, corresponding to three different strains, $\varepsilon_r = 1.00$, 1.30, and 2.01%, respectively.

3.3 XRD stress measurement after press-fitting

After press-fitting, another XRD measurement is taken. This postprocess analysis allows comparison with the prepress-fitting data to determine changes in residual stress caused by the press-fitting. The experimental methodology ensures a systematic evaluation of residual stress evolution throughout the experiment.

4. Results and Discussion

In Fig. 3(a), Pt 1 is located at the outer bottom dish, further away from the press-fitting. The residual stress increases from 4% to 17% when the strain of press-fitting increases from 1.0 to 2.01%. The effect of residual stress reduction is less significant. In Fig. 3(b), the trend of residual

Table 4
Chemical composition of pin of SUJ2 bearing steel (mass% × 100).

C	Mn	P	S	Si	Cu	Ni	Cr	Fe
101	25	0.8	0.6	23	1	2	132	Bal

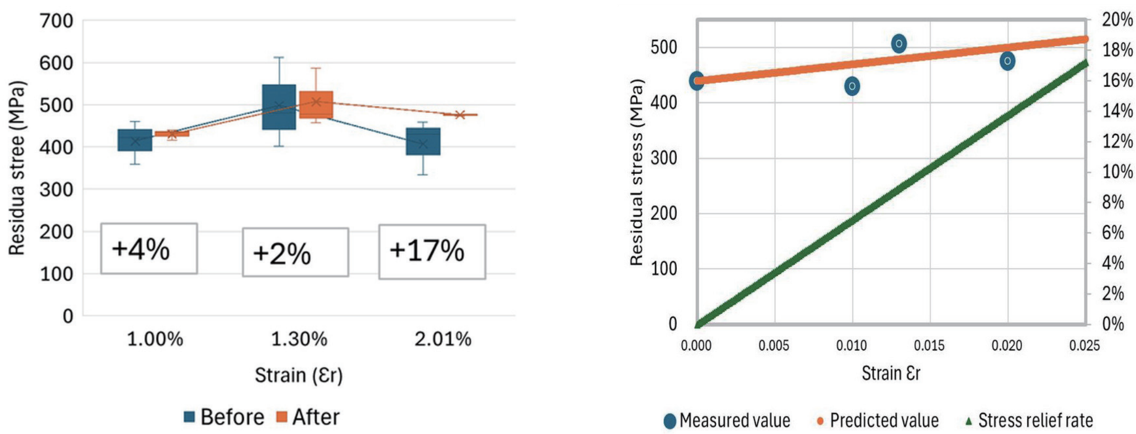

(a) (b)

Fig. 3. (Color online) (a) Changes in residual stress vs strain at Pt 1 and (b) trend of residual stress vs strain.

stress at Pt 1 shows a slight increase with increasing press-fitting strain. This suggests that the areas farther from the press-fitting zone may experience stress transmission through structural constraint or indirect deformation but without significant stress relief. The stress accumulation at these regions could be due to the redistribution of force flow through the component's geometry, indicating that residual stress is not uniformly reduced throughout the workpiece.

In Fig. 4(a), Pt 2 is at the inner bottom dish. It is closer to the press-fitting. The residual stress increases from 12 to 27%. In Fig. 4(b), Pt 2, which lies closer to the press-fitting region, shows a more pronounced increase in residual stress as strain increases. This behavior may be attributed to the transitional zone between direct deformation and the surrounding material. The residual stress here might be affected by both the press-fit expansion and the resistance from the adjacent material, creating a zone of stress concentration instead of relief. This insight is crucial for component design, suggesting that stress relief effects are not monotonic across all locations.

In Fig. 5(a), Pt 3 is on the press-fitting. At Pt 3, the residual stress decreases significantly from −45 to −67% when the strain of press-fitting increases from 1 to 2.01%. Figure 5(b) illustrates a clear and consistent trend of decreasing residual stress at Pt 3 as the strain increases. Since Pt 3 lies directly at the press-fitting interface, the applied strain is most effective here in counteracting and reducing the residual stress originally introduced by forming. This confirms that press-fitting strain has a highly localized stress-relieving effect, and the strain magnitude plays a critical role in maximizing stress reduction at the interface.

These trends provide crucial insights into the spatially dependent behavior of residual stress relief. They support the hypothesis that press-fitting is most effective near the contact zone, while its effect diminishes or even reverses further owing to complex stress redistribution.

Before press-fitting, the residual stress was found to be positive in the circumferential direction at all measured points, as presented in Table 5. This indicates that the components were subjected to compressive deformation during manufacturing processes such as plate drawing, deep-drawing, and stamping. After press-fitting, the thin-walled section undergoes radial

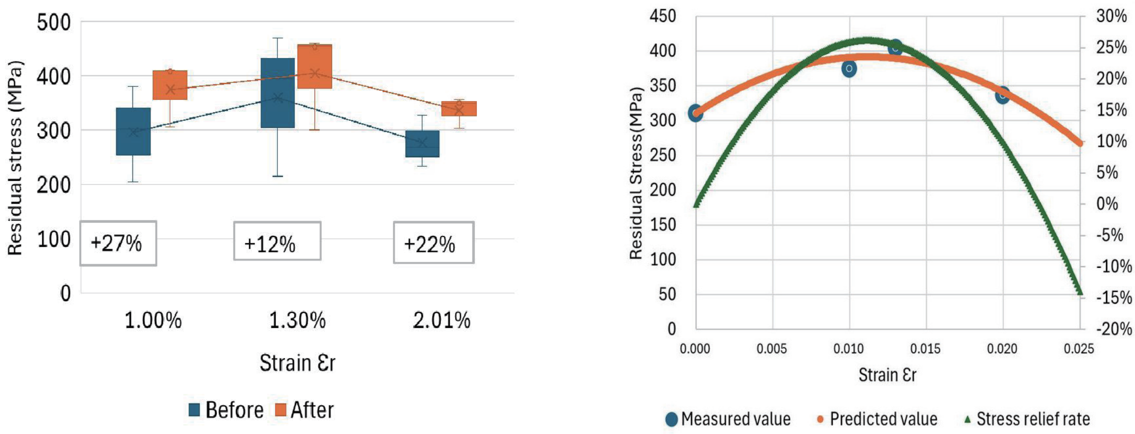

(a) (b)

Fig. 4. (Color online) (a) Changes in residual stress vs strain at Pt 2 and (b) trend of residual stress vs strain.

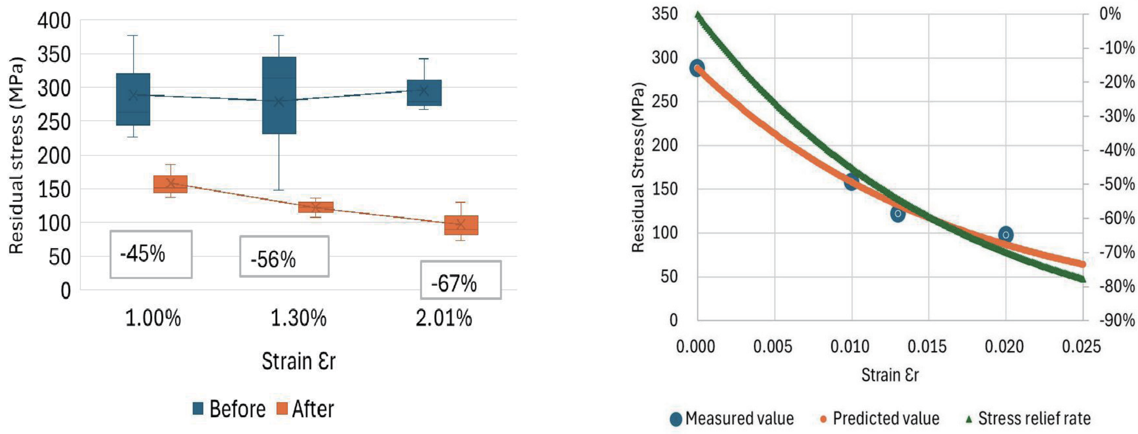

(a) (b)

Fig. 5. (Color online) (a) Changes in residual stress vs strain at Pt 3 and (b) trend of residual stress vs strain.

Table 5
Average XRD stress measurement data.

Pt 1			Pt 2			Pt 3		
			Before press-fitting					
ε_r (%)	Normal stress (MPa)	Shear stress (MPa)	ε_r (%)	Normal stress (MPa)	Shear stress (MPa)	ε_r (%)	Normal stress (MPa)	Shear stress (MPa)
1.00	414	−50	1.00	298	−56	1.00	264	−83
1.30	501	−56	1.30	340	−52	1.30	240	−74
2.01	407	−53	2.01	277	−45	2.01	296	−84
			After press-fitting					
ε_r (%)	Normal stress (MPa)	Shear stress (MPa)	ε_r (%)	Normal stress (MPa)	Shear stress (MPa)	ε_r (%)	Normal stress (MPa)	Shear stress (MPa)
1.00	430	−59	1.00	378	−49	1.00	158	−53
1.30	507	−53	1.30	405	−49	1.30	122	−45
2.01	476	−51	2.01	336	−44	2.01	197	−49

expansion, which induces circumferential tensile strain. This tensile strain counteracts the preexisting compressive stress, thereby reducing the overall residual stress in the material.

At the microscopic level, the stress above the yield strength causes plastic deformation. After external stress is removed, with elastic recovery, the uneven plastic deformation throughout the part generates residual stress. Residual stress can be measured by XRD stress measurement. At the macroscopic level, on the basis of the deformation plastic mechanics, the concept of total force and its decomposition in 3D space involves analyzing how forces acting on an object are distributed and contribute to its deformation. The total force represents the overall mechanical response of the object under external loads, encompassing all directional forces and the combined effects of internal stresses. This total force is then decomposed into components along three orthogonal axes (x, y, z), allowing for a more detailed understanding of its behavior.

Furthermore, stress distribution is analyzed by separating it into normal stress, acting along the normal direction, and shear stress, acting along the tangential direction. An additional counter stress superimposed to the workpiece can reduce residual stresses. Figure 6 shows the superposition of residual stresses at Pt3 before press-fitting [Fig. 6(a)] and after press-fitting [Fig. 6(c)].

Furthermore, Fig. 6 provides a schematic illustration of the stress evolution at Pt 3, which is directly beneath the press-fitting location. In Fig. 6(a), the initial residual stress before press-fitting shows a compressive stress field because of plastic deformation induced by the deep-drawing and stamping processes. This stress is primarily concentrated in the circumferential direction because of radial constraint and metal flow during forming.

Figure 6(b) conceptually shows the stress imposed by the press-fitting. As the rigid pin is inserted into the undersized hole, it exerts an outward radial force. This deformation produces tensile strain in the circumferential direction due to material expansion. Because the thin-walled region near the inner diameter is constrained, it undergoes localized plastic deformation while also experiencing elastic recovery in surrounding areas.

In Fig. 6(c), after press-fitting, the new residual stress distribution reflects the superposition of the original compressive stress and the tensile strain introduced by interference fitting. The result is a net reduction in circumferential residual stress at Pt 3. This confirms the mechanism of stress neutralization by deformation superposition: the externally applied press-fit stress partially cancels the preexisting internal stress, thus decreasing the overall residual stress intensity. The residual shear stress, as shown in Table 5, does not change significantly, indicating that the press-fitting primarily affects the normal stress component.

This analysis validates the concept that the localized plasticity at the interference zone is the dominant mechanism of residual stress relief. The stress redistribution follows the principles of elastic–plastic mechanics, where applied deformation beyond the yield point leads to the permanent reconfiguration of internal stress fields. In this study, we demonstrated that applying a carefully controlled interference strain can strategically reduce manufacturing-induced stress concentrations, especially in regions close to the press-fit interface.

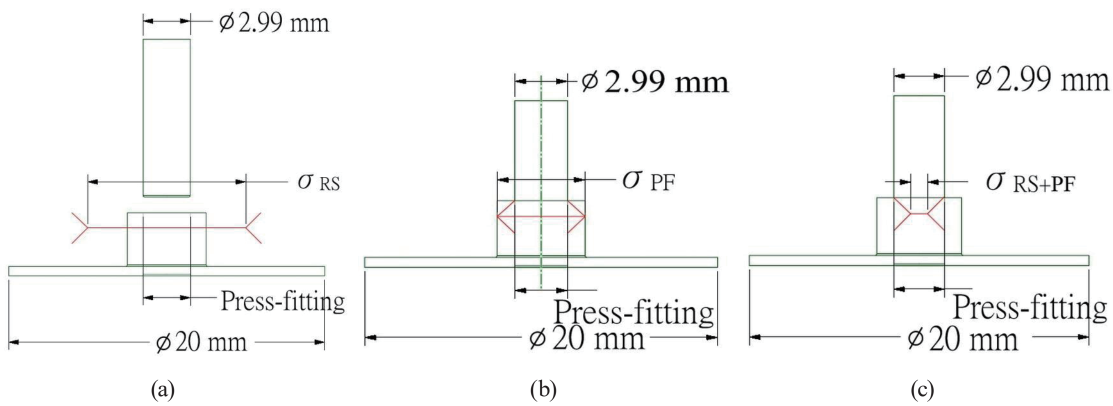

Fig. 6. (Color online) (a) Residual stress before press-fitting. (b) Stress due to press-fitting. (c) Residual stress after press-fitting.

5. Conclusions

The findings of this study reveal the significant impact of press-fitting strain on residual stress relief in deep-drawn sheet metal components. By employing a nondestructive XRD-based residual stress sensing technique, we demonstrated that varying press-fitting strains effectively modify the internal stress states of the material. Notably, significant stress reduction was observed at regions directly affected by the interference fit, while stress accumulation occurred in distant regions, indicating a complex redistribution behavior.

These insights highlight the potential of integrating mechanical processing techniques with embedded sensing technologies for advanced manufacturing. The use of XRD as a precise, nondestructive stress sensing technique enables real-time evaluation and supports the development of sensor-assisted forming and assembly processes. This approach contributes to the broader field of sensing applications in materials engineering by demonstrating how stress sensing can be utilized not only for postprocess inspection but also for process optimization and quality assurance.

Ultimately, the proposed method presents a cost-effective, sensing-integrated strategy for residual stress control, offering valuable guidance for the design and optimization of precision components in industries such as automotive, aerospace, and smart manufacturing systems. Future research may be on the exploration of the integration of real-time in-line sensing systems to further automate residual stress monitoring during production.

Acknowledgments

This work was supported by 3D-FLRS International Co., Ltd. We extend our gratitude to the team at 3D-FLRS International Co., Ltd. for their invaluable contributions, resources, and expertise, which were instrumental in the successful completion of this project. Their unwavering support and commitment to innovation considerably enhanced the quality and scope of our work. We sincerely appreciate their partnership and dedication throughout this endeavor.

The authors would also like to express their sincere appreciation to Professor Jo-Peng Tsai of CTBC University of Technology for his insightful guidance and constructive suggestions during the manuscript writing process. His academic input significantly improved the clarity and quality of this paper.

References

1 P. J. Withers and H. K. D. H. Bhadeshia: Mater. Sci. Technol. **17** (2001) 355. https://doi.org/10.1179/026708301101509980
2 D. Lohe, K.-H. Lang, and O. Vohringer: Handbook of Residual Stress and Deformation of Steel, G. Totten, M. Howes, and T. Inoue, Eds. (ASM International, Ohio, 2002) 1st ed., p. 27.
3 S. N. Shaikh: IOSR J. Mech. Eng. Civ. Eng. **3** (2016) 1. https://doi.org/10.9790/1684-15008030301-04
4 X. Deng, S. Zhang, and M. Cheng: Proc. 8th Int. Forum on Manufacturing Technology and Engineering Materials (IOP Publishing, Chongqing, 2022) 12054. https://doi.org/10.1088/1742-6596/2459/1/012054
5 N. Bastola, M. P. Jahan, N. Rangasamy, and C. S. Rakurty: Micromach. **14** (2023) 1480. https://doi.org/10.3390/mi14071480

6 Y. Yang, S. Bharech, N. Finger, X. Zhou, J. Schröder, and B.-X. Xu: npj Comput Mater. **10** (2024) 117. https://doi.org/10.1038/s41524-024-01296-5
7 X. Zheng, D. Li, W. Liao, and H. Zhang: Buildings **14** (2024) 1801. https://doi.org/10.3390/buildings14061801
8 A. H. Elsheikh, S. Shanmugan, T. Muthuramalingam, A. K. Thakur, F. A. Essa, A. M. M. Ibrahim, and A. O. Mosleh: Adv. Manuf. **10** (2022) 287. https://doi.org/10.1007/s40436-021-00371-0
9 R. Haque: Mater. Perform. Charact. **7** (2018) 956. https://doi.org/10.1520/MPC20170109
10 J. A. D. Ball, A. Kareerc, O. V. Magdysyuk, S. Michalikb, T. Connolleyb, and D. M. Collinsa: Commun. Mater. **5** (2024) 27. https://doi.org/10.1038/s43246-024-00466-8
11 I. I. Tagiltsev and A. V. Shutov: Int. J. Solids Struct. **254–255** (2022) 111924. https://doi.org/10.1016/j.ijsolstr.2022.111924
12 J. S. Robinson, R. C. Wimpory, D. A. Tanner, B. Mooney, C. E. Truman, and T. Panzner: Mater. Perform. Charact. **7** (2018) 898. https://doi.org/10.1520/MPC20170130
13 ASTM E837-20: ASTM Int. (2020). https://doi.org/10.1520/E0837-20
14 ASTM E915-21: ASTM Int. (2021). https://doi.org/10.1520/E0915-21
15 O. P. Oladijo, A. M. Venter, L. A. Cornish, and N. Sacks: Surf. Coat. Technol. **206** (2012) 4725. https://doi.org/10.1016/j.surfcoat.2012.01.044
16 E. Gorgun and M. B. Karamis: J. Mech. Sci. Technol. **33** (2019) 3231. https://doi.org/10.1007/s12206-019-0618-1
17 D. Delbergue, D. Texier, M. Lévesque, and P. Bocher: Proc. 10th Int. Conf. Residual Stress (Mater Res. Proc., Cancun, 2017) 55–60. https://doi.org/10.21741/9781945291173-10

About the Authors

Shih-Chuan Cheng received his B.E. degree in electrical engineering from the University of Queensland, Australia, in 1999 and his M.E. degree in mold and die engineering from National Kaohsiung University of Applied Sciences, Taiwan, in 2013. He is a Ph.D. candidate at the Mechanical Engineering Department of National Cheng Kung University, Taiwan. His research interests include metal forming systems, computer-aided manufacturing, and sensor applications. (n18061054@gs.ncku.edu.tw)

Rong-Shean Lee received his Ph.D. degree in mechanical engineering from the University of Leeds, U.K. From 1982 to 2019, he was a professor at National Cheng Kung University (NCKU). Since 2019, he has been Professor Emeritus at NCKU, Taiwan. His research interests include metal forming systems, computer-aided manufacturing, applied plasticity, and intelligent manufacturing. (mersl@mail.ncku.edu.tw)